The complicating role of pnictogen bond formation in the solution-phase and solid-state structures of the heavier pnictogen atranes.

Shiva Moaven,[†] *Olivia H. Villanueva,*[†] *Daniel K. Unruh, Anthony F. Cozzolino**

Department of Chemistry and Biochemistry, Texas Tech University, 1204 Boston Avenue, Lubbock, TX 79409-1061, United States

Electronic Supplementary Information

Table of Contents

S1 Experimental Details

S1.1 General Methods

The starting materials, antimony (III) ethoxide (Alfa Aesar, 98%), antimony trichloride (99% Strem), triethanolamine (Alfa Aesar, 98%), tri-*iso*-propanolamine (Alfa Aesar, 95%), were used as purchased. Antimony tris-*tert*-butoxide was prepared based on our previous report.[1] Anhydrous tetrahydrofuran was obtained by passing HPLC grade tetrahydrofuran over a bed of activated molecular sieves in a commercial (LC Technologies Solutions Inc.) solvent purification system (SPS). Deuterated solvents, purchased from Cambridge Isotopes Laboratory, were degassed using three freeze-pump-thaw cycles before being transferred onto freshly activated molecular sieves. Air sensitive manipulations were performed in an N_2 purged inert atmosphere box (LC Technology Solutions Inc.). All NMR spectra were collected on a JEOL ECS 400 MHz NMR spectrometer. All IR spectra were obtained using a Nicolet iS-5 FT-IR spectrometer equipped with a Specac Di Quest ATR accessory, and CHN analysis were obtained on-site with a Perkin Elmer 2400 Series II CHNS/O analyzer or through Micro-Analysis, Inc.

S1.2 Synthesis

S1.2.1 Preparation of macrocyclic tetramer of Sb-**1**: (Sb-**1**)$_4$

Triethanolamine (149 mg, 1.00 mmol) was dissolved in 5 mL of anhydrous THF and 2 mL solution containing 341 mg (1.00 mmol) antimony(III) *tert*-butoxide was added to the stirring solution of the alcohol. Upon addition of the antimony reagent rapid formation of a white solid was observed. The white solid was filtered and washed with THF. PXRD of the recovered solid confirmed phase purity of the compound. Yield: 141 mg (52.6%, 0.53 mmol). mp = 250-255 °C. ^{1}H NMR (400 MHz, Chloroform-*d*, δ ppm) 2.63-2.99 (m, 24H), 4.07-4.14 (2 × s, 24H). ^{13}C NMR (100.6 MHz,

Chloroform-*d*, δ ppm) Sb-**1**: 53.44, 58.70; (Sb-**1**)$_4$: 56.55, 57.04, 62.04, 62.96. *Di*-ATR-FTIR (cm^{-1}): 2891, 2845 (s, ν_{C-H}) 1080, 1032, 1010 (vs, ν_{C-O}) 528, 496, 459 (m and s, $\nu_{Sb-O/N}$). Anal. Calc. for $C_{24}H_{48}N_4O_{12}Sb_4$: C, 26.90; H, 4.51; N, 5.23. Found: C, 26.57; H, 4.46; N, 5.35.

S1.2.2 Synthesis of (Sb-**2**)$_3$

Tri-*iso*-propanolamine (191 mg, 1.00 mmol) was dissolved in 5 mL of anhydrous THF. Antimony(III) ethoxide (257 mg, 1.00 mmol) was dissolved in 2 mL anhydrous THF, and then added to the stirring solution of tri-*iso*-propanolamine and was stirred for 1 hour at room temperature. All volatiles were removed under vacuum to give a white solid. Yield: 146 mg (47%, 0.47 mmol). mp = 93-106 °C. ^{1}H NMR (400 MHz, Chloroform-*d,* δ ppm) 1.21 (m, 9H), 2.17-3.21 (m, 6H), 3.90-4.60 (m, 3H). ^{13}C NMR (100.6 MHz, Chloroform-*d*, δ ppm) Sb-**2** 22.20, 60.18, 63.77 (Sb-**2**)$_3$ 21.96, 22.30, 23.79, 63.15, 64.07, 66.66, 67.56, 68.18, 69.37. *Di*-ATR-FTIR (cm^{-1}): 2959, 2923, 2962, 2826 (s, ν_{C-H}), 1039 (s, ν_{C-O}) 536, 467 (m, ν_{Sb-O}). Anal. Calc. for $C_{27}H_{54}N_3O_9Sb_3$: C, 34.87; H, 5.85; N, 4.52. Found: C, 34.68.; H, 5.95; N, 4.53.

S1.3 X-ray Diffraction

S1.3.1 Single-crystal X-ray diffraction

Data were collected on a Bruker PLATFORM three circle diffractometer equipped with an APEX II CCD detector and operated at 1350 W (40kV, 30 mA) to generate (graphite monochromated) Mo Kα radiation (λ = 0.71073 Å). Crystals of (Sb-**2**)$_3$ were transferred from the vial and placed on a glass slide in polyisobutylene. A Zeiss Stemi 305 microscope was used to identify a suitable specimen for X-ray diffraction from a representative sample of the material. The crystal and a small amount of the oil were collected on a MīTiGen cryoloop and transferred to the instrument where it was placed under a cold nitrogen stream (Oxford) maintained at 100 K throughout the duration of the experiment. The sample was optically centered with the aid of a

video camera to ensure that no translations were observed as the crystal was rotated through all positions.

A unit cell collection was then carried out. After it was determined that the unit cell was not present in the CCDC database a sphere of data was collected. Omega scans were carried out with a 60 sec/frame exposure time and a rotation of 0.50° per frame. After data collection, the crystal was measured for size, morphology, and color. These values are reported in Table 1.

After data collection, the unit cell was re-determined using a subset of the full data collection. Intensity data were corrected for Lorentz, polarization, and background effects using the Bruker program APEX 3. A semi-empirical correction for adsorption was applied using the program *SADABS*.[2] The *SHELXL-2014*,[3] series of programs was used for the solution and refinement of the crystal structure. Hydrogen atoms bound to carbon atoms were located in the difference Fourier map and were geometrically constrained using the appropriate AFIX commands. The rigid-bond restraint RIGU was applied globally and reflections 100, 010, and −101 were omitted due to being behind the arm of the beamstop.

Table S1. Crystal data and structure refinement for (Sb-**1**)$_4$ and (Sb-**2**)$_3$.

Structure	(Sb-**1**)$_4$	(Sb-**2**)$_3$
Crystal Color	colorless	colorless
Crystal Habit	cube	hexagonal plate
Empirical formula	$C_{24}H_{48}N_4O_{12}Sb_4$	$C_{27}H_{54}N_3O_9Sb_3$
Formula weight (g/mol)	1071.66	929.98
Temperature	100(2) K	100(2) K
Wavelength	0.71073 Å	0.71073 Å
Crystal system	Monoclinic	Triclinic
Space group	$P2_1/c$	$P\bar{1}$
Unit cell dimensions	a = 13.3095(14) Å b = 11.5424(12) Å c = 12.4332(13) Å α = 90° β = 117.620(10)° γ = 90°	a = 12.661(3) Å b = 13.388(4) Å c = 13.591(6) Å α = 118.198(6)° β = 107.187(6)° γ = 101.120(4)°
Volume	1692.4(3) Å^3	1781.9(10) Å^3
Z	2	2
Calculated density	2.103 g/cm^3	1.733 g/cm^3
Absorption coefficient	3.221 mm^{-1}	2.307 mm^{-1}
F(000)	1040	924
Crystal size	0.145 × 0.120 × 0.045 mm	0.085 × 0.065 × 0.015 mm
Theta range for data collection	1.727 to 27.215°	1.901 to 25.545°
Limiting indices	−17≤ h ≤17 −14≤ k ≤14 −16≤ l ≤15	−15≤ h ≤13 −16≤ k ≤16 −16≤ l ≤16
Reflections collected / unique	19551/3767 [R(int) = 0.0252]	27274/6622 [R(int) = 0.0660]
Completeness to theta = 25.242°	100.0%	99.8%
Refinement method	Full-matrix least-squares on F^2	Full-matrix least-squares on F^2
Data / restraints / parameters	3767/0/199	6622/387/388
Goodness-of-fit on F^2	1.030	0.967
Final R indices [I>2sigma(I)]	R1 = 0.0167, wR2 = 0.0386	R1 = 0.0390, wR2 = 0.0602
R indices (all data)	R1 = 0.0203, wR2 = 0.0402	R1 = 0.0704, wR2 = 0.0678
Largest diff. peak and hole	0.545 and −0.359 e·Å^{-3}	0.727 and −0.692 e·Å^{-3}

S1.3.2 Powder X-ray Diffraction

The diffraction patterns for Sb-**1** and Sb-**2** were collected on a Rigaku Ultima III powder diffractometer. X-ray diffraction patterns were obtained by using a 2θ scan with the source fixed at 0° and the detector scanning a θ range of 5-60°, step size = 0.02°, and scan time of 10 min/degree. The X-ray source was Cu Kα radiation (λ=1.5418 Å) with an anode voltage of 40 kV and a current of 44 mA. The beam was then discriminated by Rigaku's Cross Beam parallel beam optics to create a monochromatic parallel beam. Diffraction intensities were recorded on a scintillation detector after being filtered through a Ge monochromator.

Samples of Sb-**1** and Sb-**2** were packed inside borosilicate capillaries with inner diameter of 0.3 mm and wall thickness of 0.01 mm purchased from Charles Supper Company. Samples were prepared under inert atmosphere and the tubes were sealed with grease. After sealing they were mounted on a capillary holder and data was collected. The resulting diffractograms were processed with the software JADE v9.1. Simulated patterns were obtained from single crystal data of each sample using the Mercury 3.10 software and the appropriate X-ray wavelength.

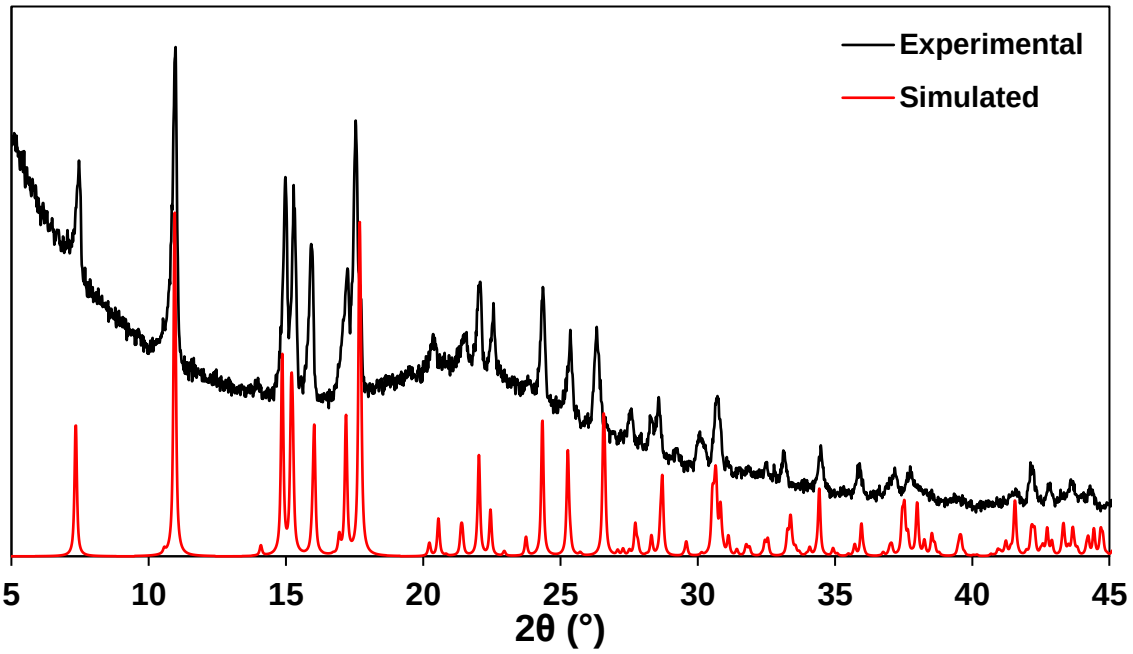

Figure S1. Powder x-ray diffraction of Sb-**1** (in black) and the simulated powder pattern of (Sb-**1**)$_4$ (in red) from the single crystal structure.

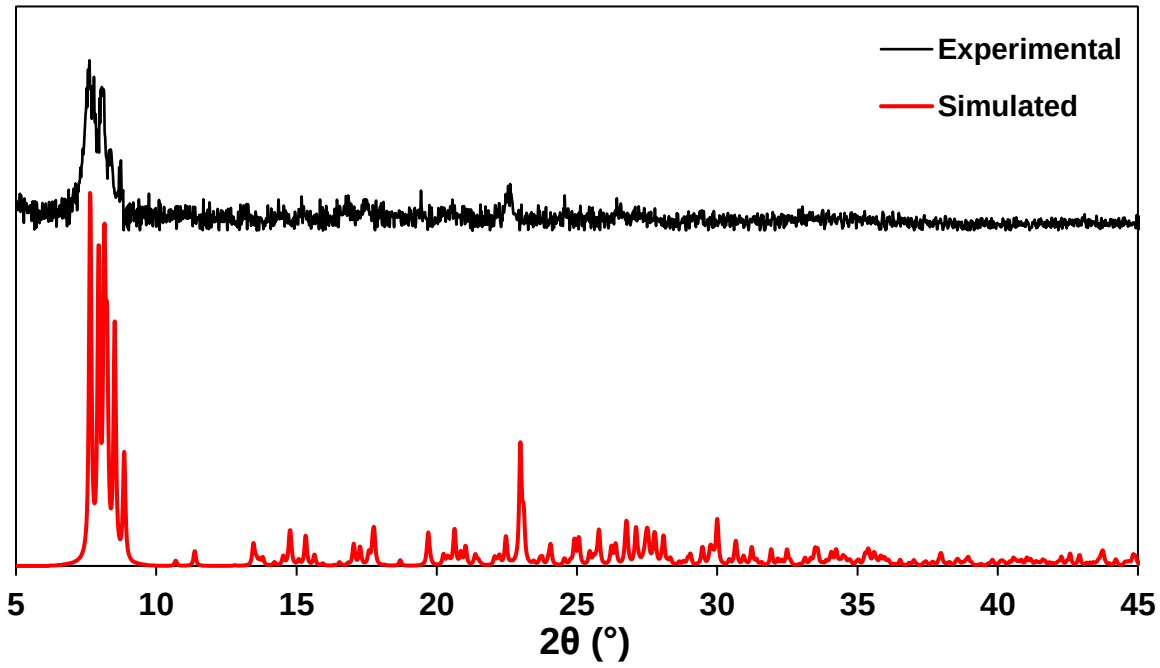

Figure S2. Powder x-ray diffraction of Sb-**2** (in black) and the simulated powder pattern of (Sb-**2**)$_3$ (in red) from the single crystal structure.

Sb-**1** (2.7 mg, 0.01 mmol) was sealed under vacuum in a glass tube (1 cm diameter), wrapped in aluminum foil, and sublimed at 483 K in a Kugelrhor glass oven with an approximately 1.5 inches of the covered tube left out of the distillation apparatus. The tube was then turned around, placed entirely in the apparatus, and the temperature of the apparatus was lowered to 453 K to allow for slow sublimation and crystal growth. Crystals of Sb-**2** (3.1 mg, 0.01 mmol) were grown by sublimation in a Kugelrhor glass oven, as described above, starting at 453 K.

Data were collected on a Bruker PLATFORM three circle diffractometer equipped with an APEX II CCD detector and operated at 1350 W (40kV, 30 mA) to generate (graphite monochromated) Mo Kα radiation (λ = 0.71073 Å). Crystals of Sb-**1** and Sb-**2** were transferred from the tube and placed on a glass slide in polyisobutylene. A Zeiss Stemi 305 microscope was used to identify a suitable specimen of each for X-ray diffraction from a representative sample of the material. The crystals and a small amount of the oil were collected on a MiTiGen cryoloop and transferred to the instrument. The sample was optically centered with the aid of a video camera to ensure that no translations were observed as the crystal was rotated through all positions.

A unit cell collection was then carried out. A consistent unit cell was not obtained for the sublimed material of Sb-**1**. A powder x-ray diffraction (PXRD) of the material was collected and differs from the collected PXRD of (Sb-**1**)$_4$ (Figure S3.) The unit cell of crystals of sublimed Sb-**2** were a match with (Sb-**2**)$_3$ grown from solution.

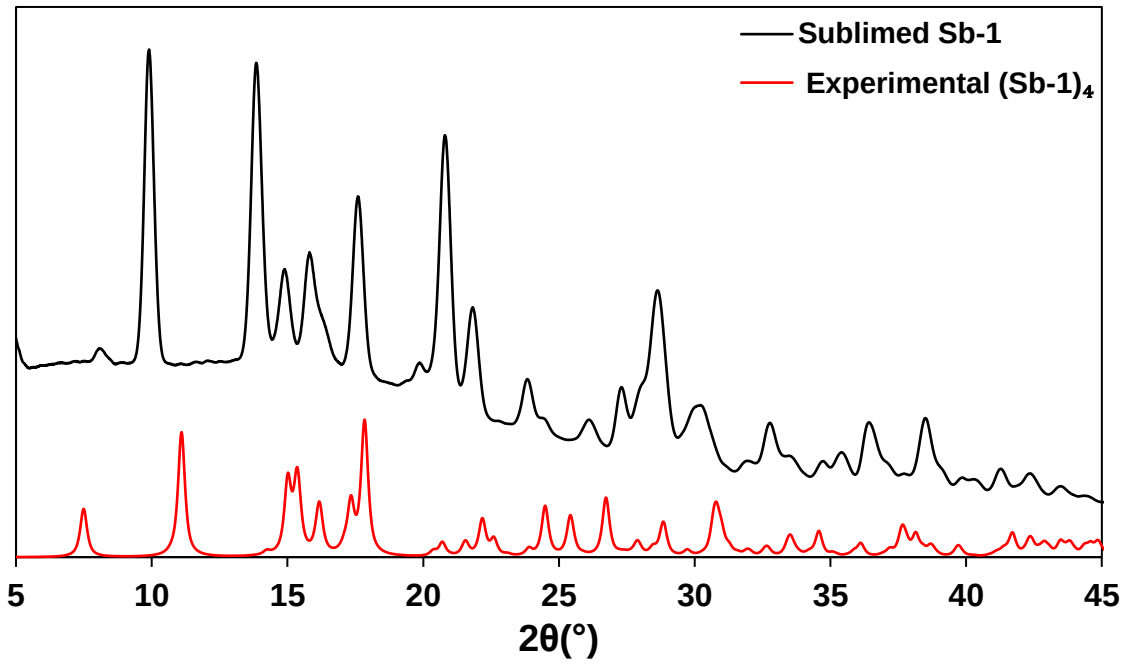

Figure S3. Powder x-ray diffraction of single crystals from sublimed Sb-**1** (in black) and experimental (Sb-**1**)$_4$ (in red).

S1.4 Computational Methods

Calculations were performed using the ORCA 4.0 quantum chemistry program package from the development team at the Max Planck Institute for Bioinorganic Chemistry.[4] Starting geometries for optimizations were from relevant crystal structures. Minima were confirmed by comparing energies of different isomers and performing a frequency calculation to ensure that all frequencies are positive. The lowest energy structures that are discussed contained only positive vibrational frequencies. All calculations were carried out using the Zero-Order Regular Approximation (ZORA).[5,6] For geometry optimizations, frequencies, and thermochemistry the B97-D3[7] functional and def2-TZVPP[8,9] with SARC/J basis sets[10] were used for hydrogen atoms and all other atoms respectively. Spin-restricted Kohn–Sham determinants[11] were chosen to describe the closed shell wavefunctions, employing the RI approximation[12] and the tight SCF convergence criteria provided by ORCA. The basis set superposition error (BSSE) was corrected using the Boys and Bernardi procedures.[13] The cartesian coordinates of the geometry optimized molecules and supramolecules are provided as .xyz files in a .zip file. Molecular volumes were estimated using MultiWFN.[14]

Table S2. DFT calculated energies for gas phase monomer and dimer of Sb-**1**.

	S (E_h)	*H* (E_h)	*G* (E_h)	ZPE (E_h)	E_{Disp} (E_h)
Sb-**1**	−0.04820	−7092.47781	−7092.52602	0.18763	−0.07741
$(Sb\text{-}\mathbf{1})_2$	−0.07475	−14184.97723	−14185.05198	0.37640	−0.18087

$$2\ Sb\text{-}\mathbf{1} \rightleftharpoons (Sb\text{-}\mathbf{1})_2 \quad \text{(S1)}$$

$$\Delta S_{Rxn} = \left(S_{(Sb\text{-}\mathbf{1})_2} - 2S_{Sb\text{-}\mathbf{1}}\right) \quad \text{(S2)}$$

$$\Delta H_{Rxn} = \left(H_{(Sb\text{-}\mathbf{1})_2} - 2H_{Sb\text{-}\mathbf{1}}\right) - BSSE^{*} \quad \text{(S3)}$$

$$\Delta G_{Rxn} = \left(G_{(Sb\text{-}\mathbf{1})_2} - 2G_{Sb\text{-}\mathbf{1}}\right) \quad \text{(S4)}$$

$$ZPE_{Rxn} = \left(ZPE_{(Sb\text{-}\mathbf{1})_2} - 2ZPE_{Sb\text{-}\mathbf{1}}\right) \quad \text{(S5)}$$

$$E_{Disp_{Rxn}} = \left(DC_{(Sb\text{-}\mathbf{1})_2} - 2DC_{Sb\text{-}\mathbf{1}}\right) \quad \text{(S6)}$$

*BSSE of (Sb-**1**)$_2$ is -9.70166 kJ·mol^{-1}

Table S3. Energetics of the reaction for the gas phase monomer-dimer equilibrium, according to equations S1-S6.

	ΔS_{Rxn} (kJ·mol^{-1}·K^{-1})	ΔH_{Rxn}[a] (kJ·mol^{-1})	ΔG_{Rxn}[a] (kJ·mol^{-1})	ZPE_{Rxn} (kJ·mol^{-1})	$E_{Disp_{Rxn}}$ (kJ·mol^{-1})
2 Sb-**1** ⇌ (Sb-**1**)$_2$	0.19081	−47.02980	0.13114	2.97978	−68.37105

a) ZPE_{Rxn} and $E_{Disp(Rxn)}$ are included.

S1.5 Spectroscopic Data

S1.5.1 NMR Spectra

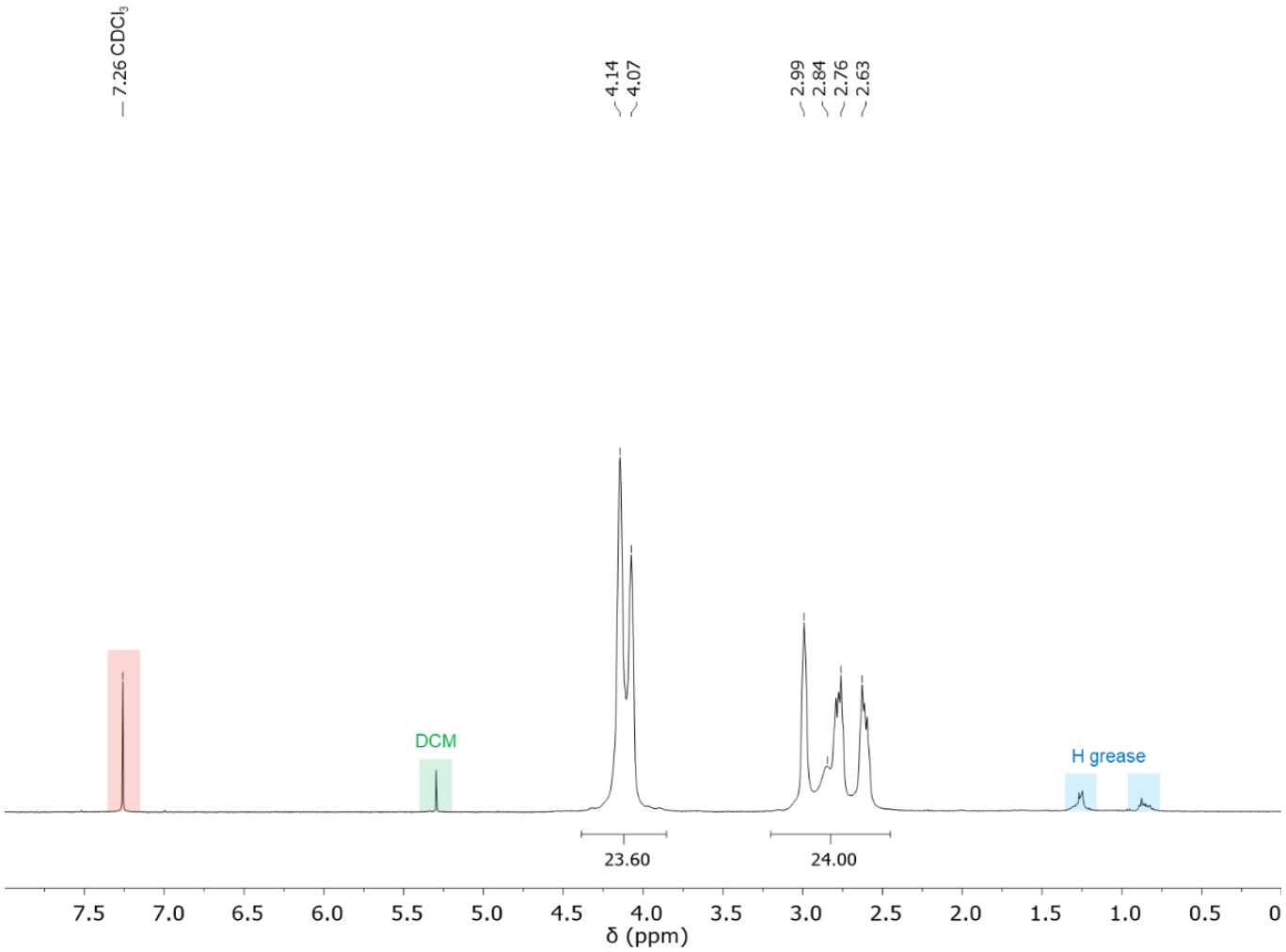

Figure S4. ^{1}H NMR of Sb-**1** in chloroform-*d*.

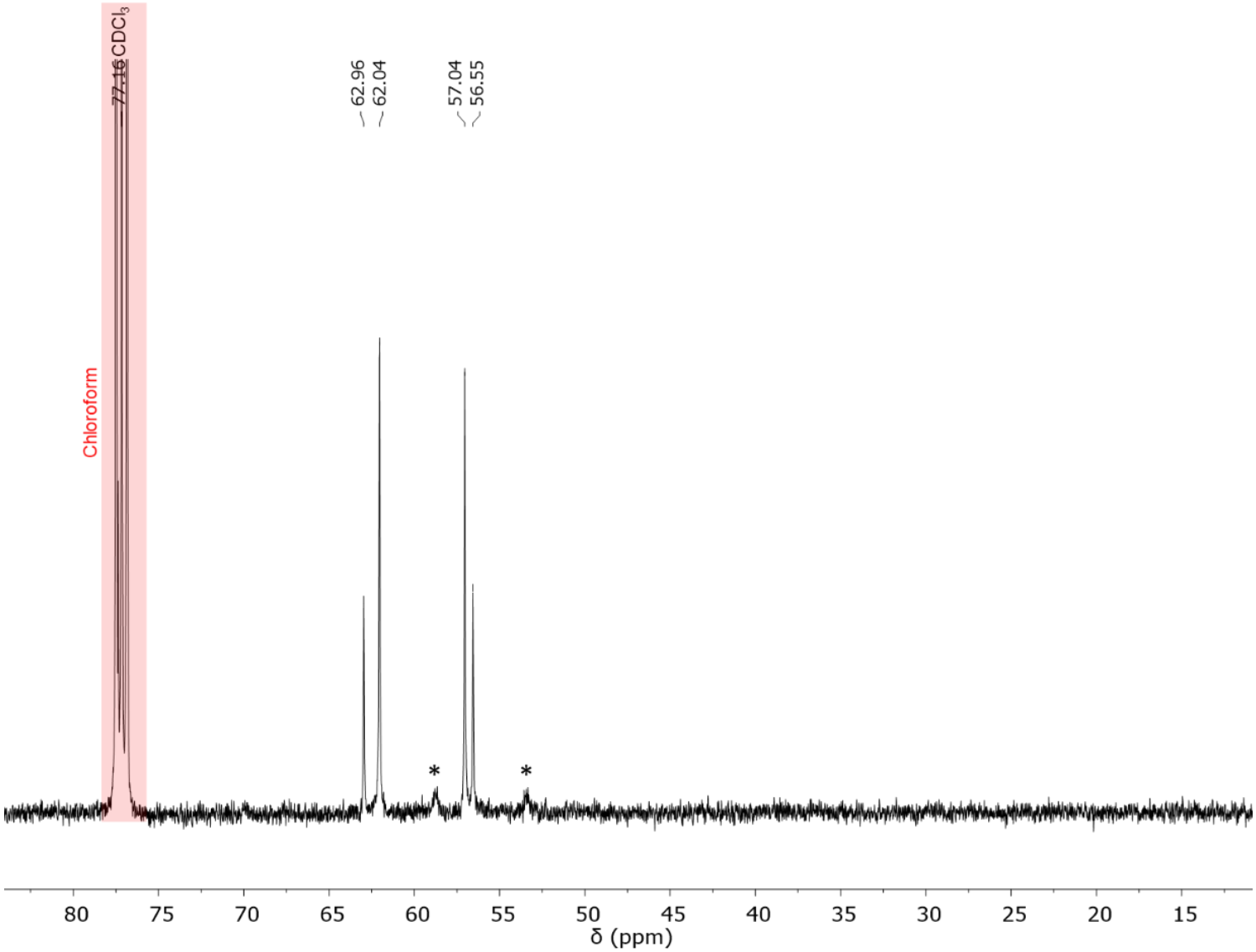

Figure S5. $^{13}C\{^{1}H\}$ NMR of Sb-**1** in chloroform-*d*,* denotes signals of putative monomeric stibatrane.

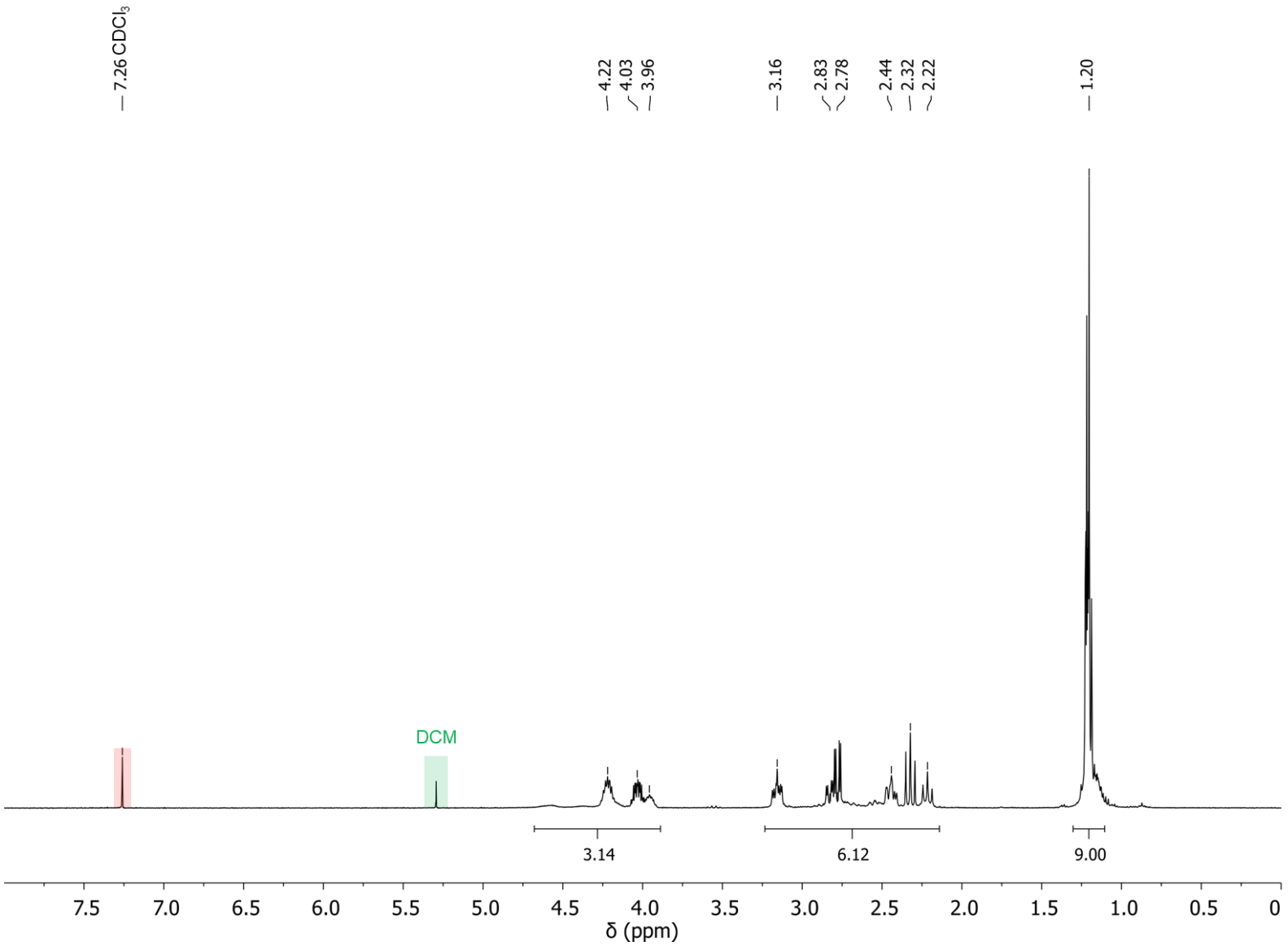

Figure S6. ^{1}H NMR of Sb-**2** as synthesized in chloroform-*d*.

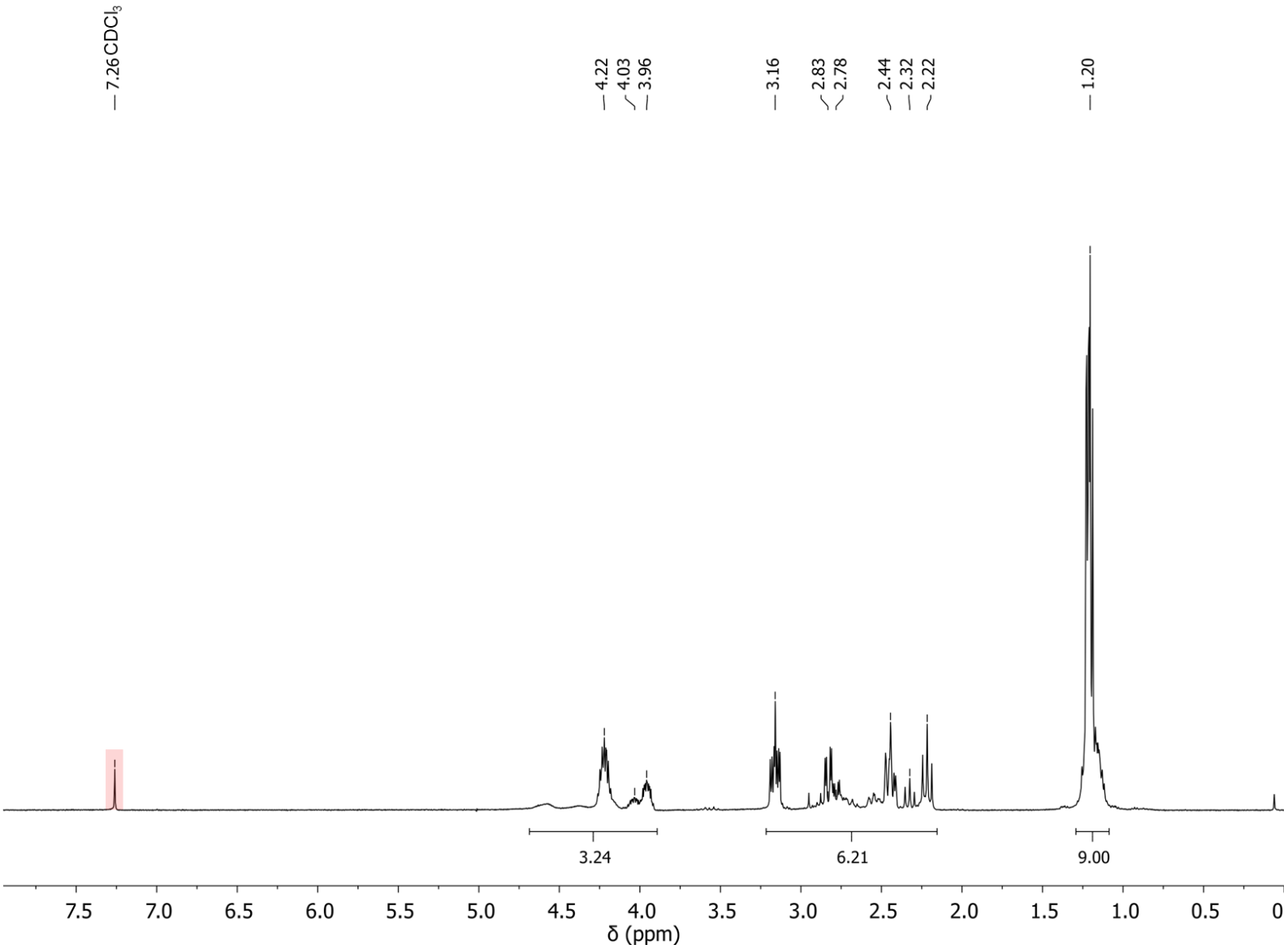

Figure S7. ^{1}H NMR of Sb-**2** recrystallized from dimethylformamide in chloroform-*d*.

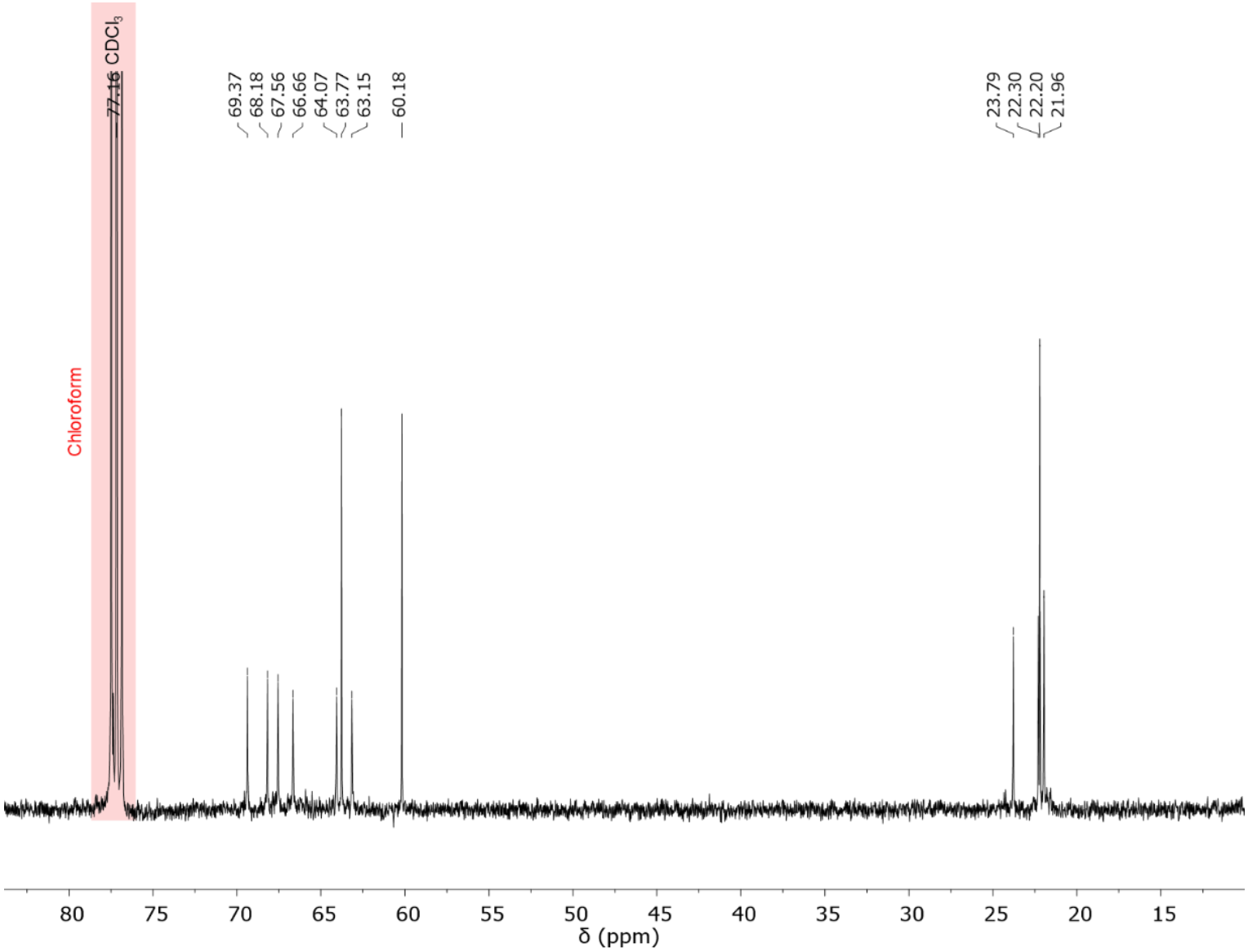

Figure S8. $^{13}C\{^{1}H\}$ NMR of Sb-**2** in chloroform-*d*.

S1.5.2 Equilibrium studies

All NMR measurements for equilibrium studies were obtained on a JEOL ESC 400 MHz NMR spectrometer in chloroform-*d* solutions at 296, 313, 323, and 333 K. Three samples of Sb-**1**: 2.7 mg (0.010 mmol), 5.4 mg (0.020 mmol), and 10.7 mg (0.0399 mmol), were dissolved in 1.00 mL of chloroform-*d*. Peaks were fit with Laurentian functions to obtain integrated areas from overlapping peaks. Areas of signals associated with either monomer or oligomer were combined, and concentrations were determined based on the ratio of intensities (normalized to the number of protons). The equilibrium constant, K_{eq}, was determined from the ratio of monomer and oligomer according to eq. 1 and 2.

Table S4. Dimer and monomer concentration of Sb-1 and K_{eq} as a function of temperature for 10 mM total solution concentration				
Concentration (mM)	**Temperature (K)**	**[(Sb-1)$_2$]**	**[Sb-1]**	**K_{eq}**
10	**296**	**4.8×10^{-3}**	**5.2×10^{-3}**	**180**
10	**313**	**4.0×10^{-3}**	**6.0×10^{-3}**	**110**
10	**323**	**3.1×10^{-3}**	**6.9×10^{-3}**	**64**
10	**333**	**1.7×10^{-3}**	**8.3×10^{-3}**	**24**

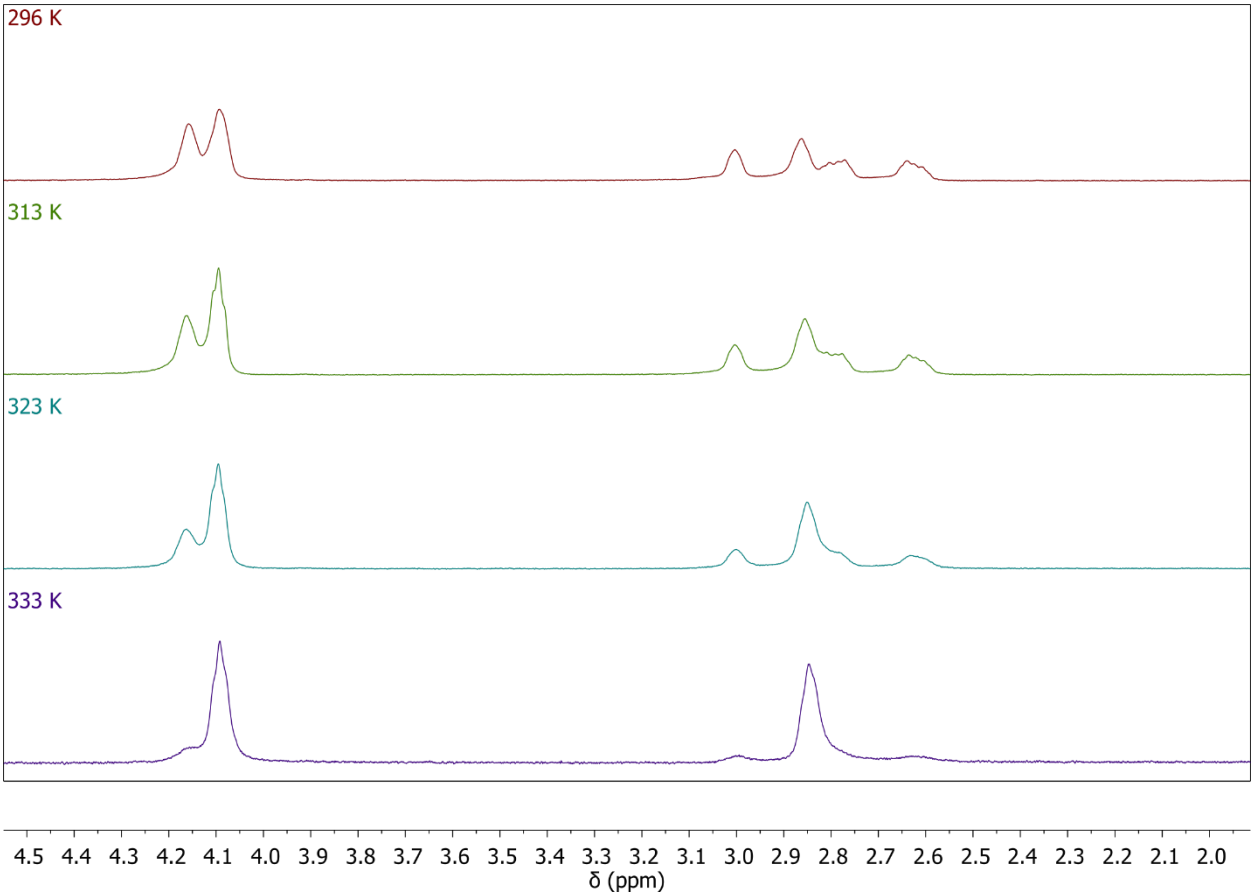

Figure S9. ^{1}H NMR spectra of 10 mM Sb-**1** chloroform-*d* solution as a function of temperature.

Table S5. Dimer and monomer concentration of Sb-1 and K_{eq} as a function of temperature for 20 mM total solution concentration				
Concentration (mM)	**Temperature (K)**	**[(Sb-1)$_2$]**	**[Sb-1]**	**K_{eq}**
20	**296**	**1.2×10^{-2}**	**8.1×10^{-3}**	**180**
20	**313**	**9.8×10^{-3}**	**1.0×10^{-2}**	**95**
20	**323**	**7.8×10^{-3}**	**1.2×10^{-2}**	**53**
20	**333**	**4.4×10^{-3}**	**1.6×10^{-2}**	**18**

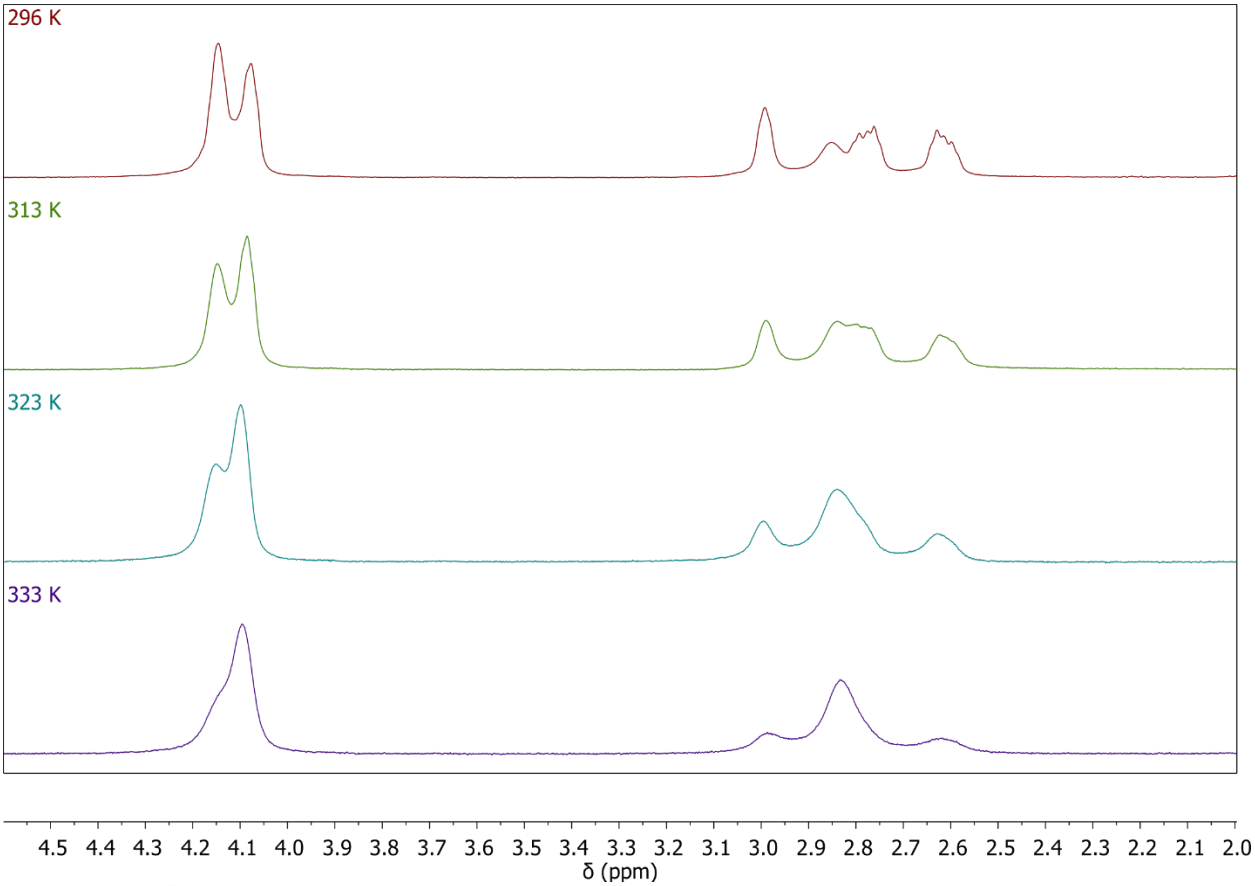

Figure S10. ^{1}H NMR spectra of 20 mM Sb-**1** chloroform-*d* solution as a function of temperature.

Table S6. Dimer and monomer concentration of Sb-1 and K_{eq} as a function of temperature for 39.9 mM total solution concentration				
Concentration (mM)	**Temperature (K)**	**[(Sb-1)$_2$]**	**[Sb-1]**	***K*$_{eq}$**
39.9	**296**	**2.75×10^{-2}**	**1.25×10^{-2}**	**174**
39.9	**313**	**2.49×10^{-2}**	**1.51×10^{-2}**	**109**
39.9	**323**	**1.96×10^{-2}**	**2.04×10^{-2}**	**47.0**
39.9	**333**	**1.43×10^{-2}**	**2.57×10^{-2}**	**21.8**

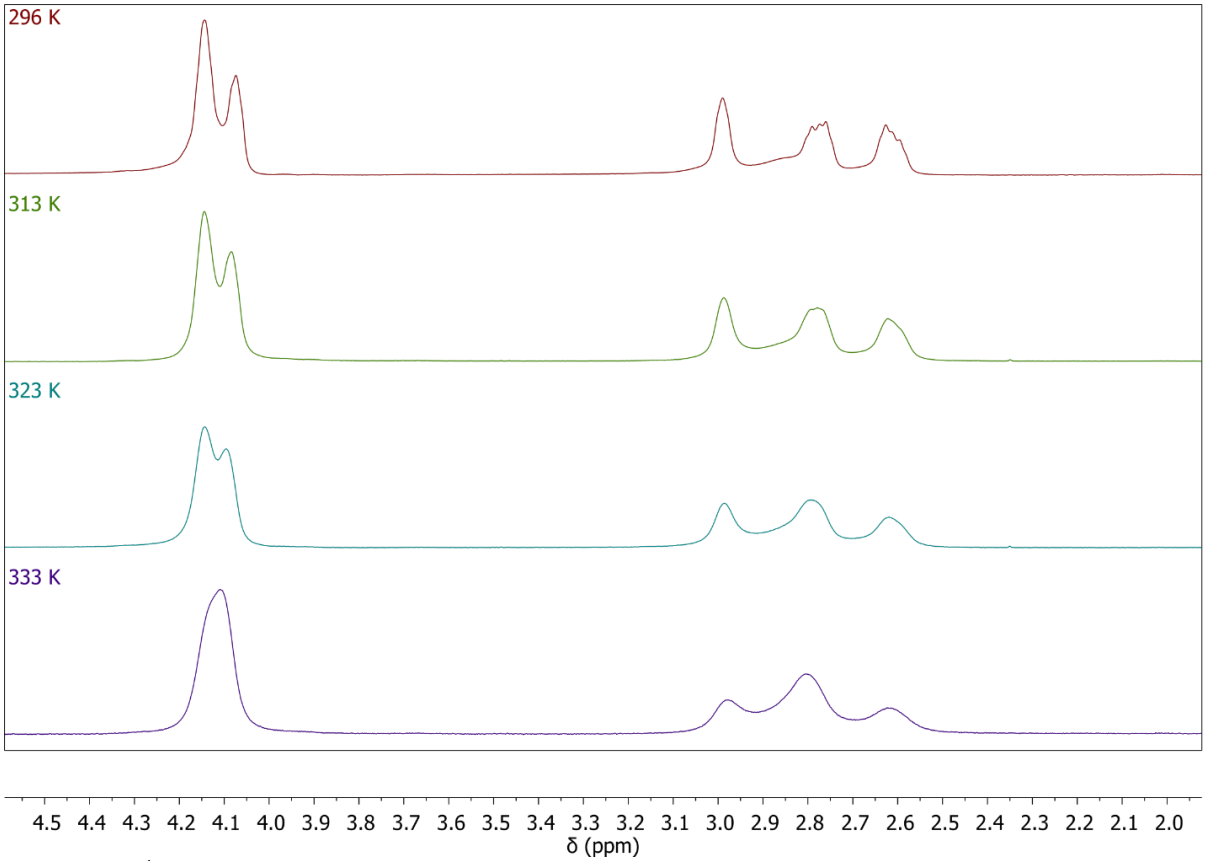

Figure S11. ^{1}H NMR spectra of 39.9 mM Sb-**1** chloroform-*d* solution as a function of temperature.

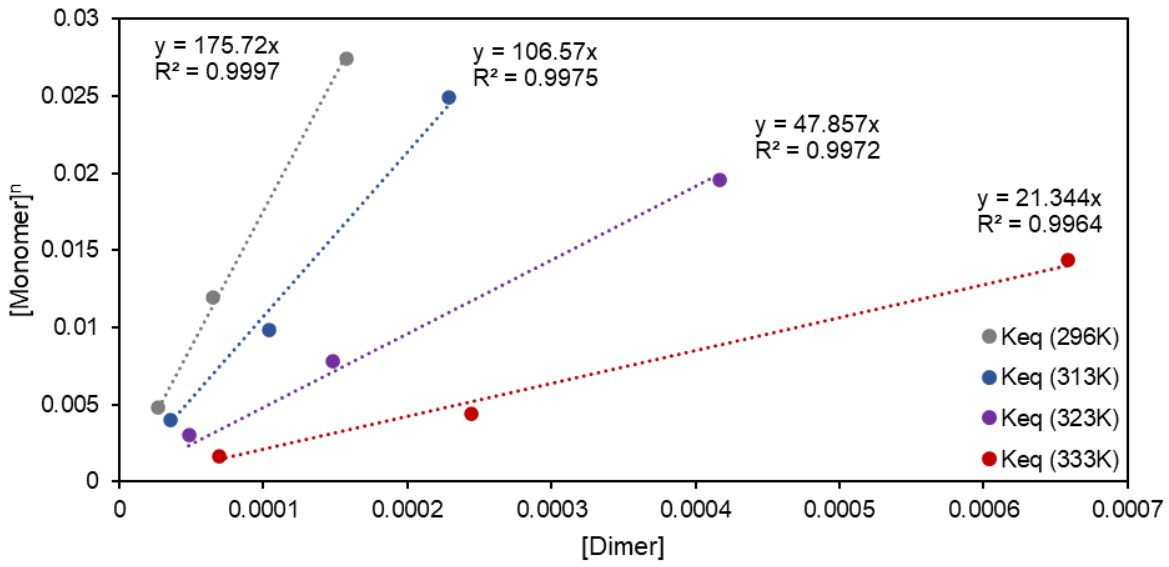

Figure S12. Equilibrium constant determination plot for monomer-dimer relationship (eq 2, n = 2) of Sb-**1** in chloroform-*d* solution.

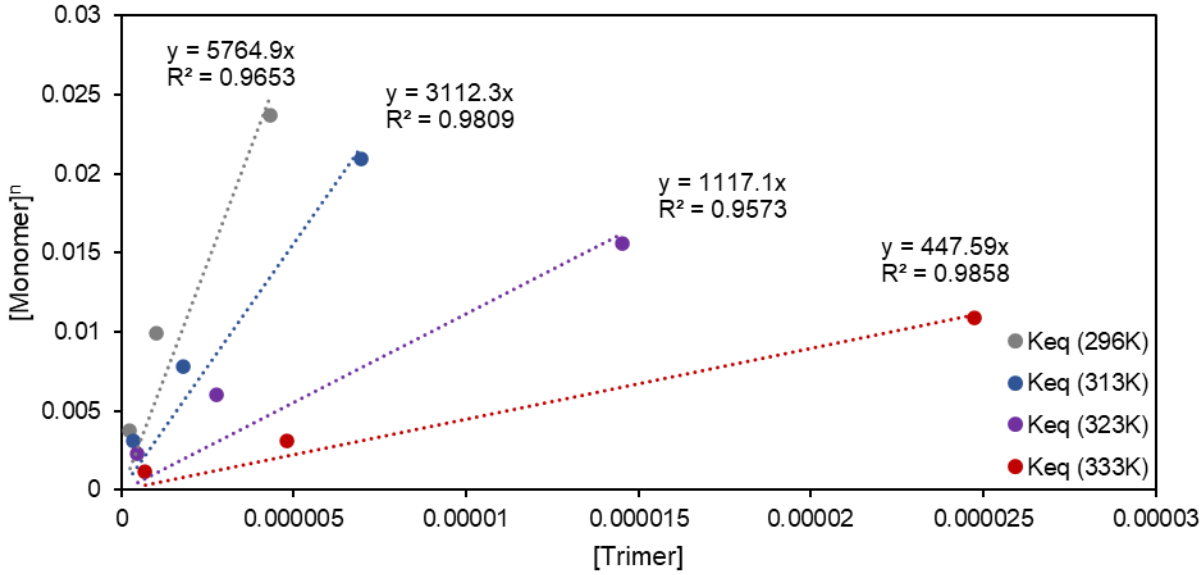

Figure S13. Equilibrium constant determination plot for a monomer-trimer relationship (eq 2, n = 3) of Sb-**1** in chloroform-*d* solution.

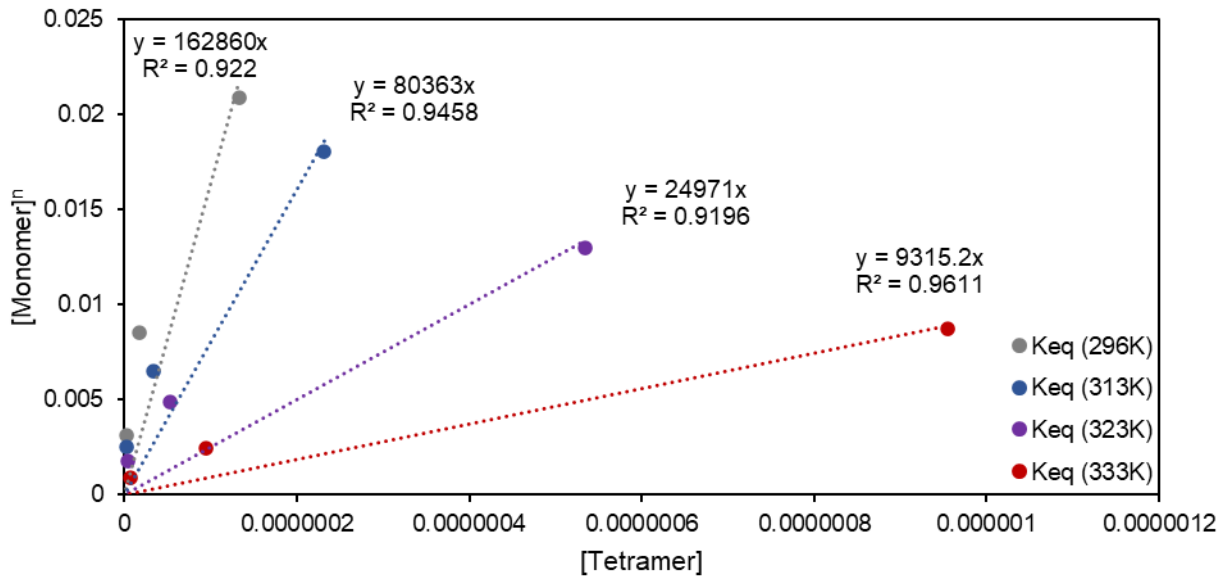

Figure S14. Equilibrium constant determination plot for a monomer-tetramer relationship (eq 2, n = 4) of Sb-**1** in chloroform-*d* solution.

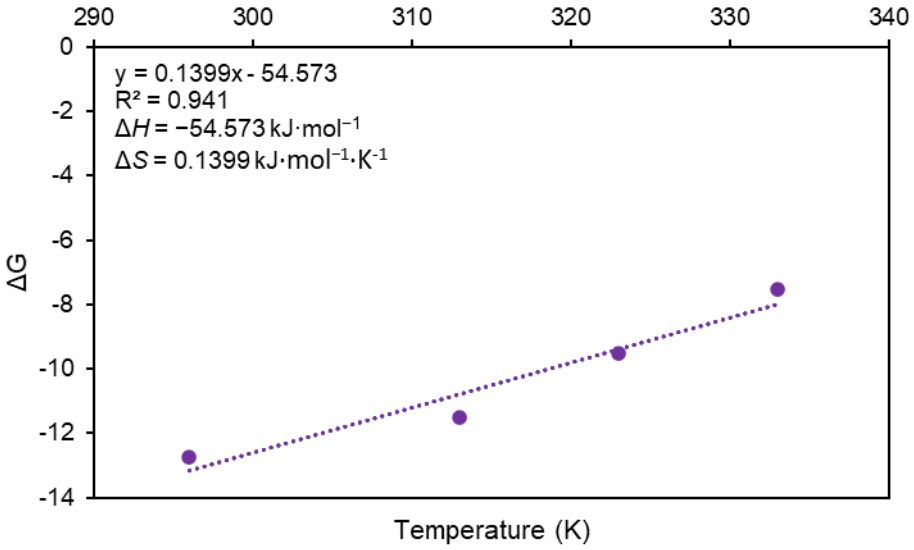

Figure S15. van't Hoff plot for Sb-**1** determined from equilibrium constants as evaluated in Figure S11.

S1.5.3 Pulsed-field gradient spin echo (PFGSE) NMR spectroscopy

All diffusion coefficient measurements were obtained on a JEOL ESC 400 MHz NMR spectrometer in chloroform-*d* solution at 296 K. Spectra from the simulated spin-echo attenuation of the ^{1}H diffusion in the solution were collected with 21 gradient values from 300 to 2500 G·m^{-1}, applied during δ = 2 ms, and diffusion delay times of 100 ms for 10 mM and 39.9 mM samples of Sb-**1**. Diffusion curves were obtained from the integrated values based on the highest value. These values were fit with a diffusion model using the GRG Nonlinear engine of the Solver package in Microsoft Excel.

Diffusion model for calculation of diffusion coefficient is represented by equation S7

$$I(g)=I_0 e^{-D(\gamma g\delta)^2(\Delta-\frac{\delta}{3})} \quad \text{(S7)}$$

where I_0 is the reference spin-echo intensity in the absence of gradient, D is the diffusion constant, γ is the ^{1}H gyromagnetic ratio, g is gradient strength, Δ delay time.[15]

Stokes-Einstein equation, equation S8, where D is the diffusion constant, k_B is Boltzmann constant, T is temperature in Kelvin, η is solvent viscosity (a value of 0.539 mPa·s for chloroform at 296 K was used),[16] r is hydrodynamic radii.

$$D=\frac{k_B T}{6\pi\eta r} \quad \text{(S8)}$$

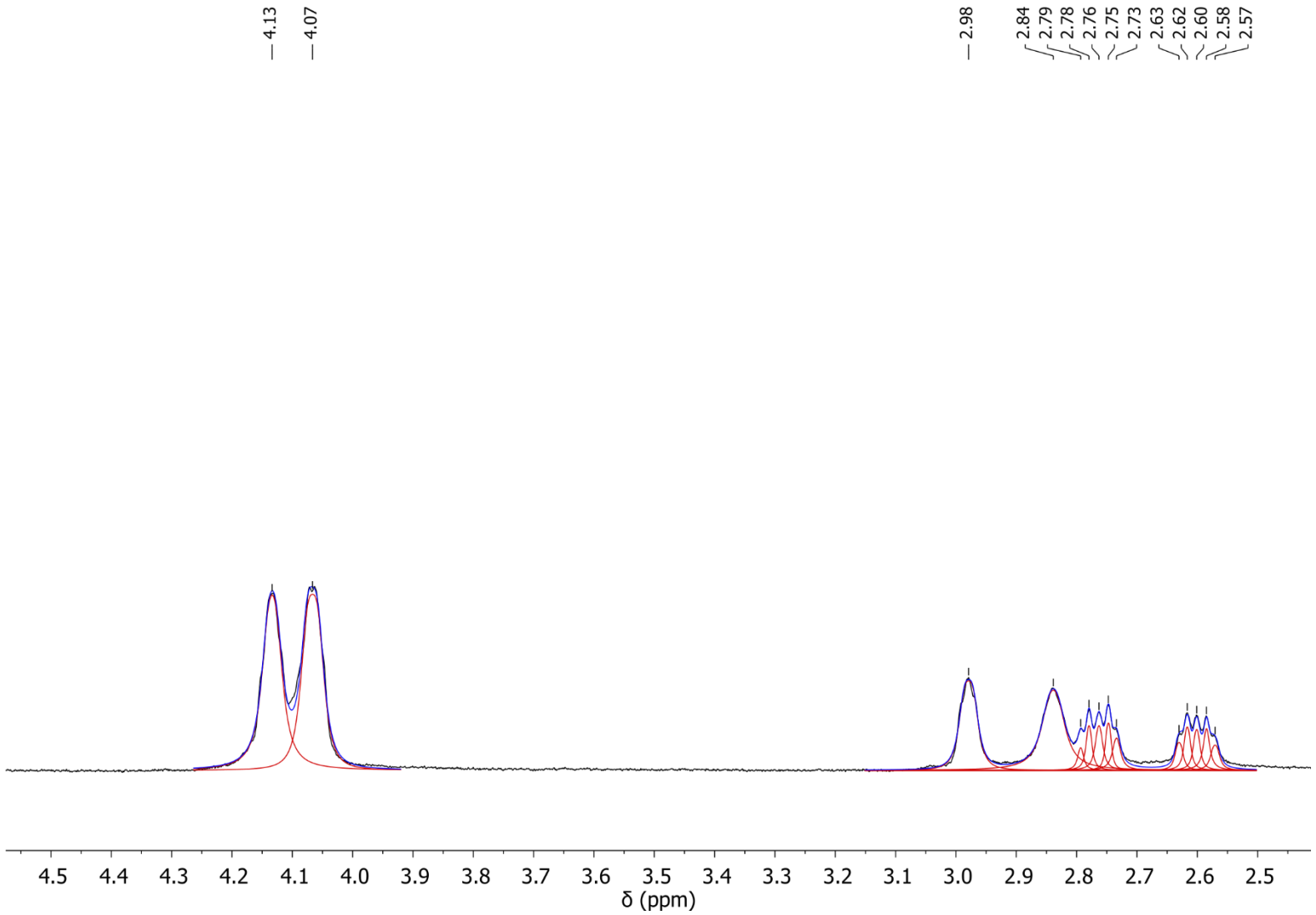

Figure S16. Fitting of data from PFGSE experiment for Sb-**1**.

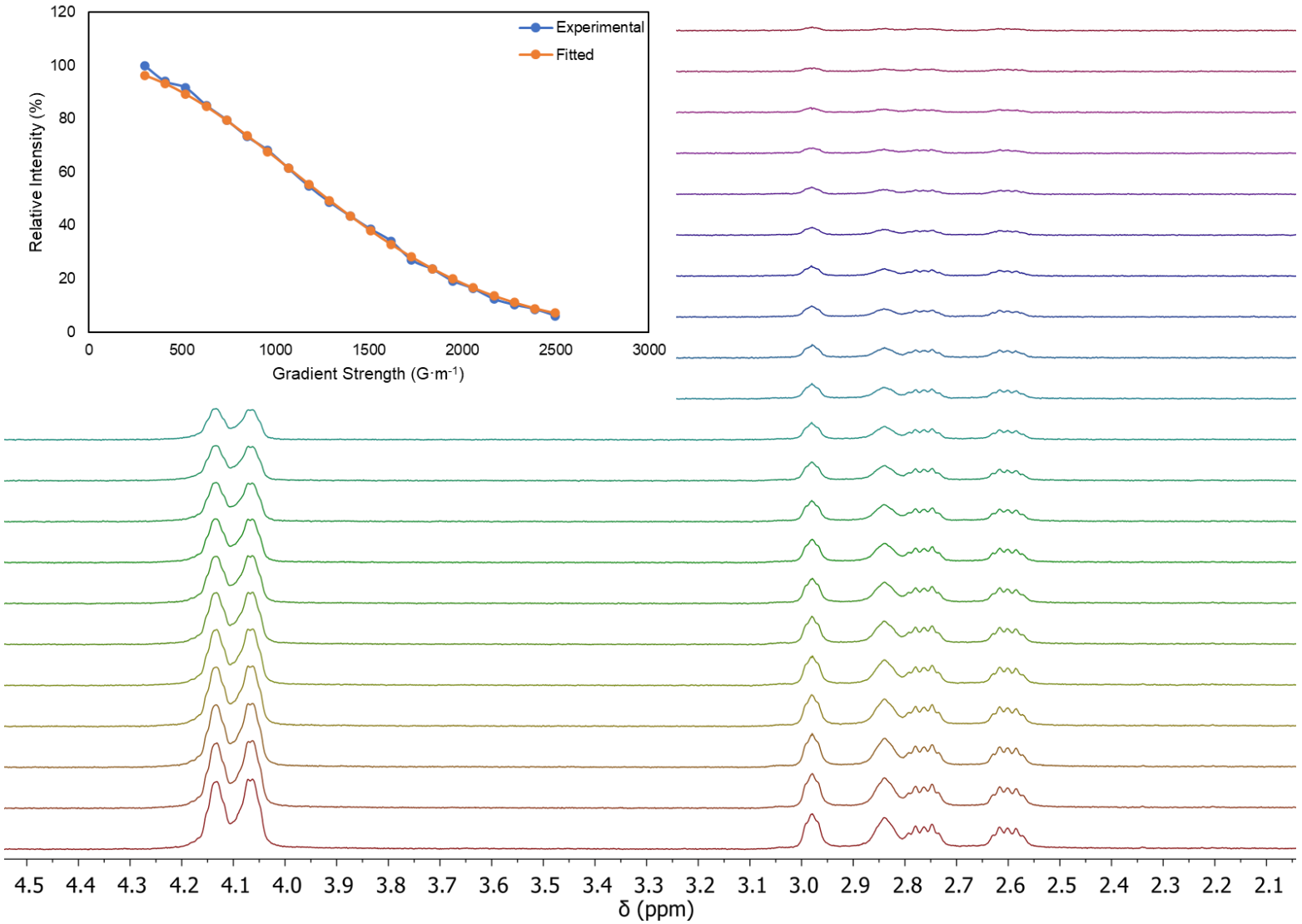

Figure S17. PFGSE spectra of 10 mM Sb-**1** chloroform-*d* solution at 296 K with insert of data fitting of diffusion curves for the peak at 2.84 ppm, representing monomer.

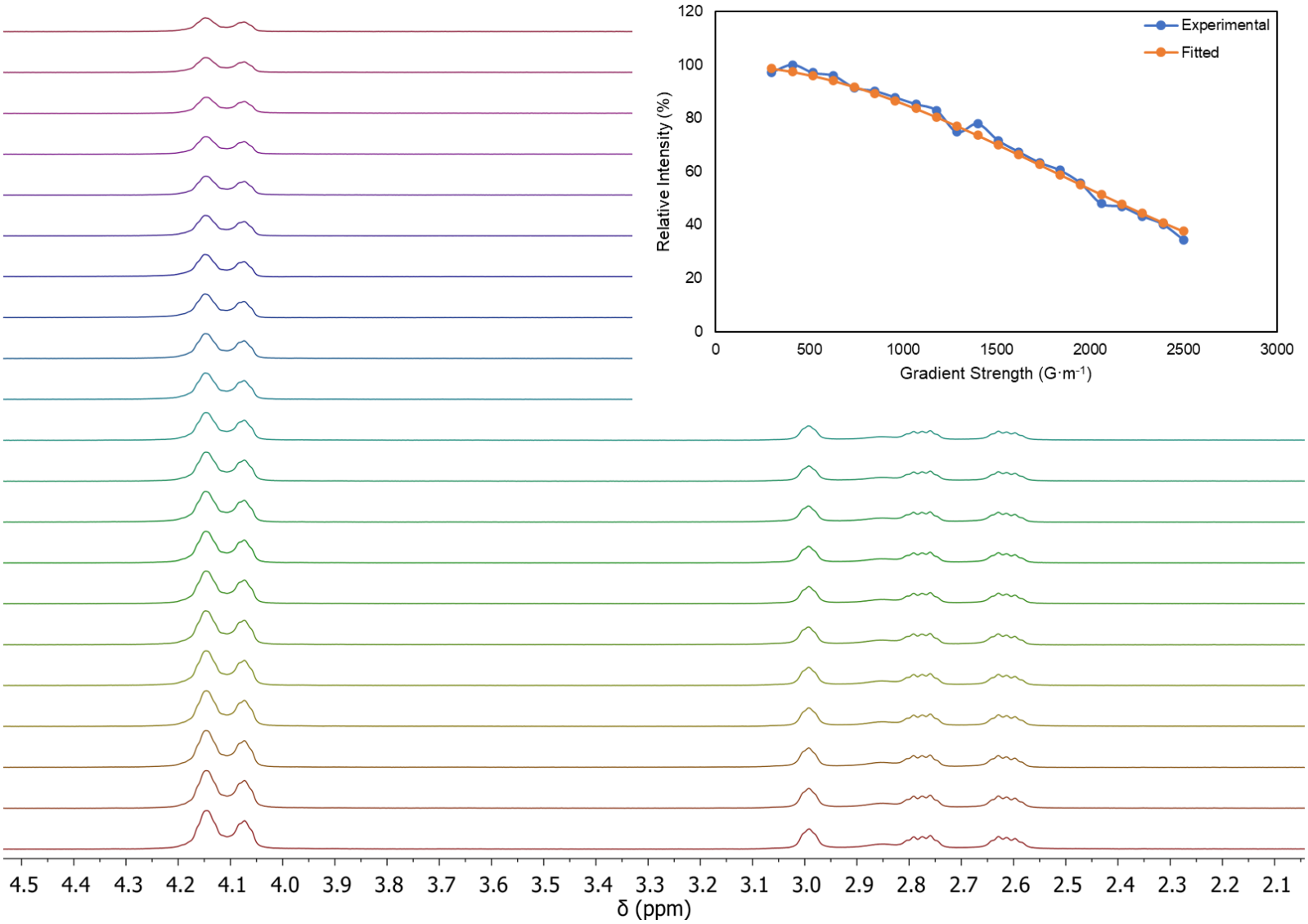

Figure S18. PFGSE spectra of 39.9 mM Sb-**1** chloroform-*d* solution at 296 K with insert of data fitting of diffusion curves for the peak at 4.14 ppm, representing dimer.

S1.5.4 Di-ATR-FTIR

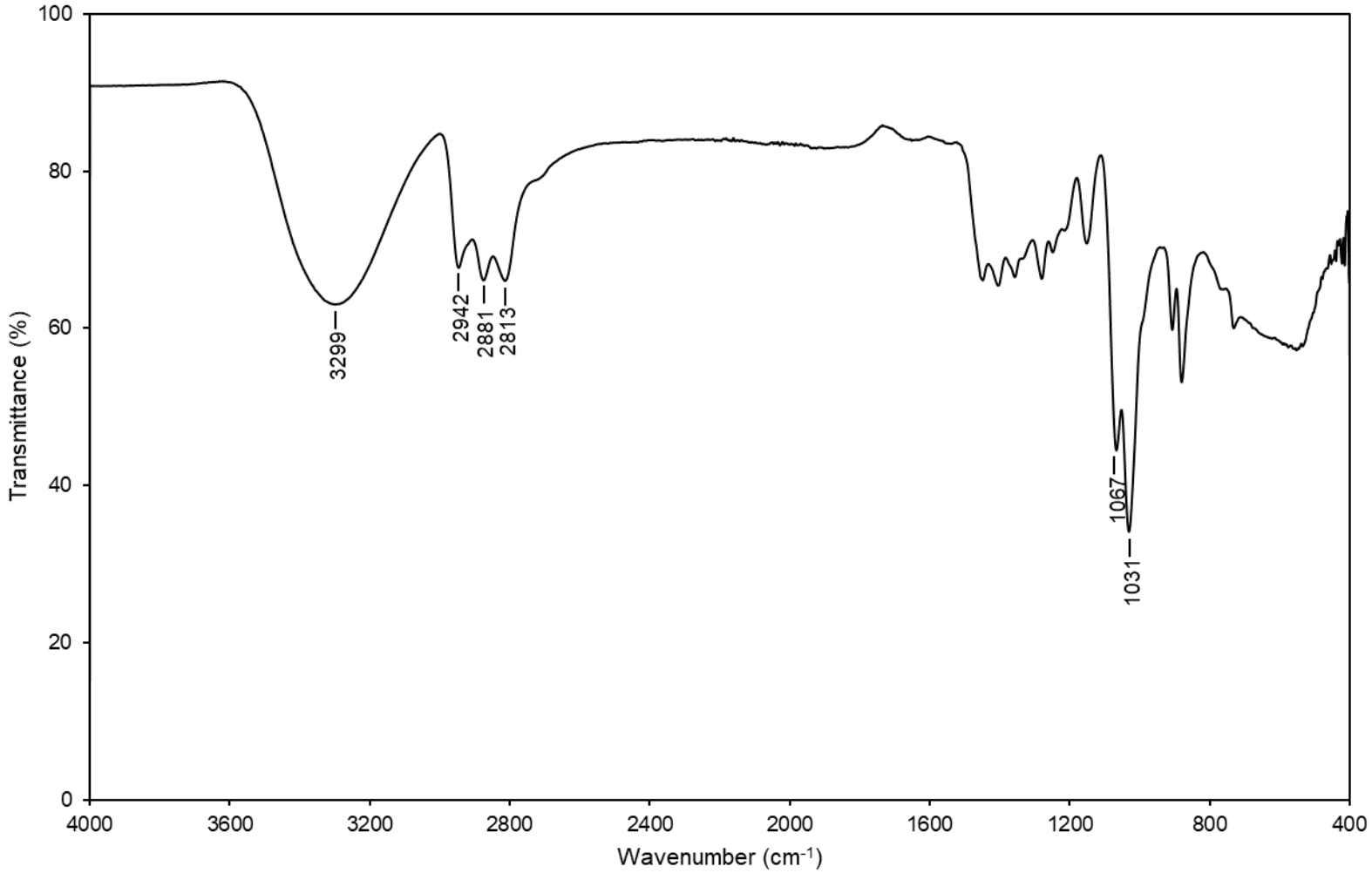

Figure S19. Di-ATR-FTIR triethanolamine (H_3-**1**).

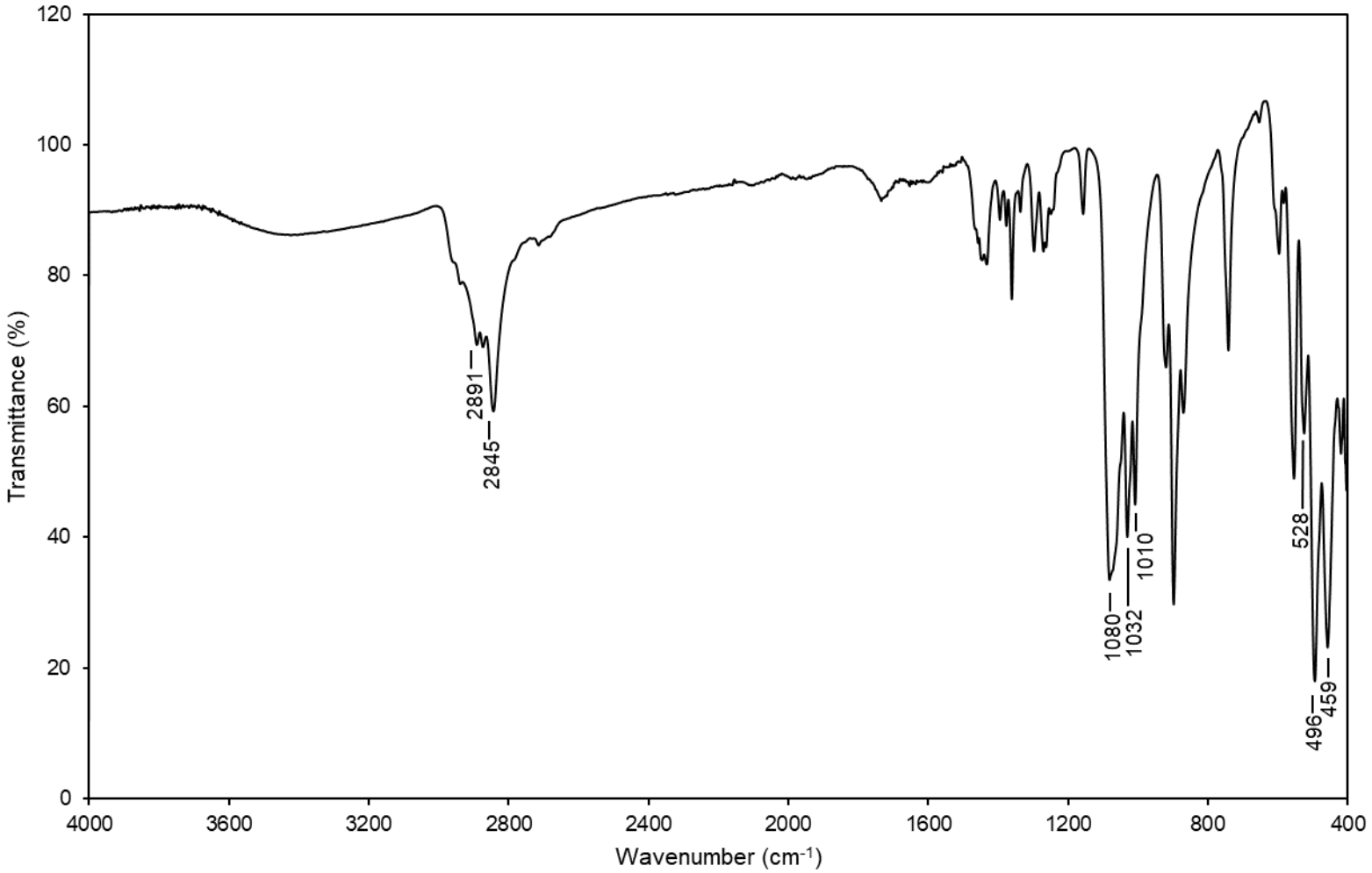

Figure S20. Di-ATR-FTIR Sb-**1**.

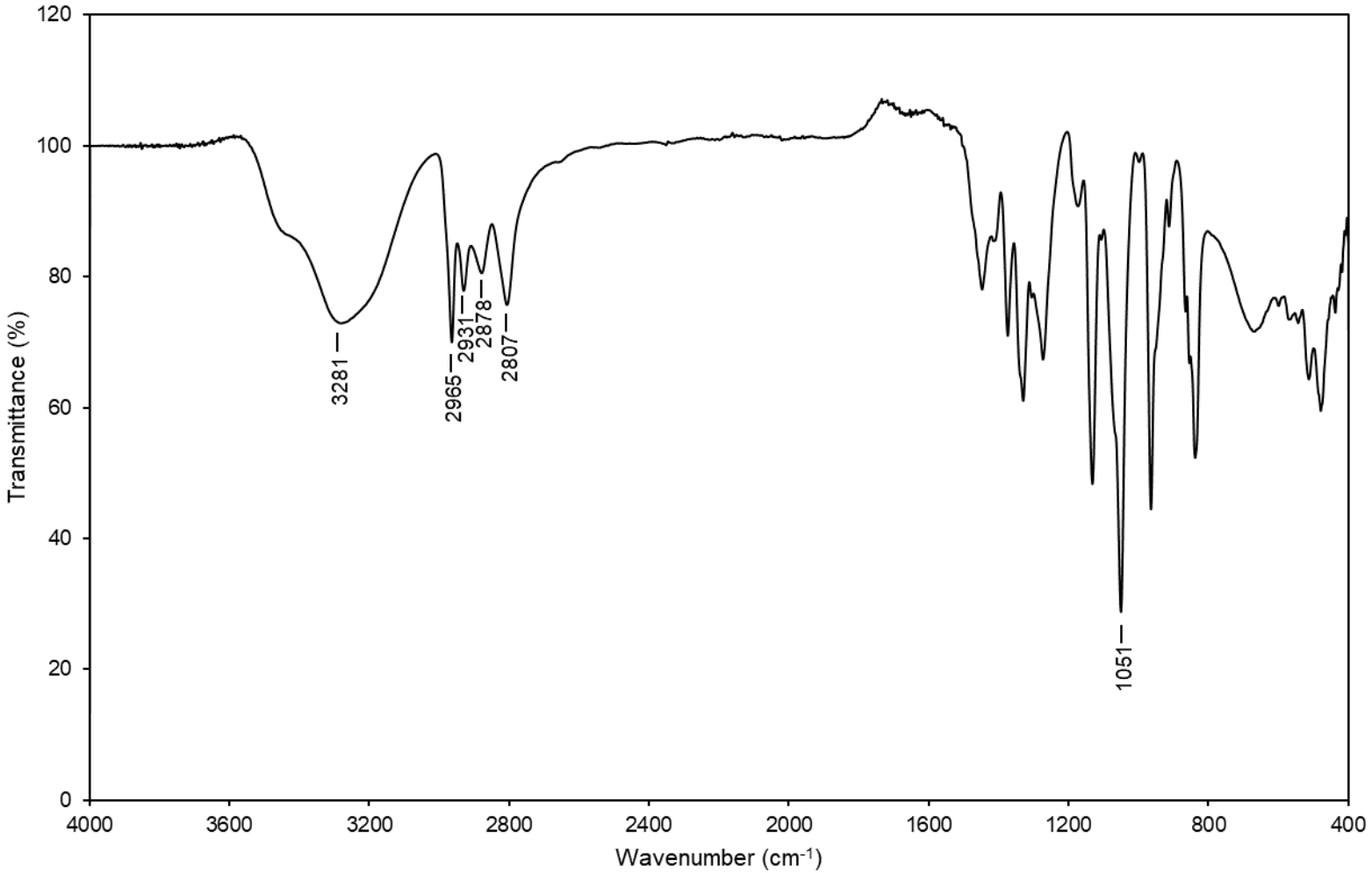

Figure S21. Di-ATR-FTIR tri-*iso*-propanolamine (H_3-**2**).

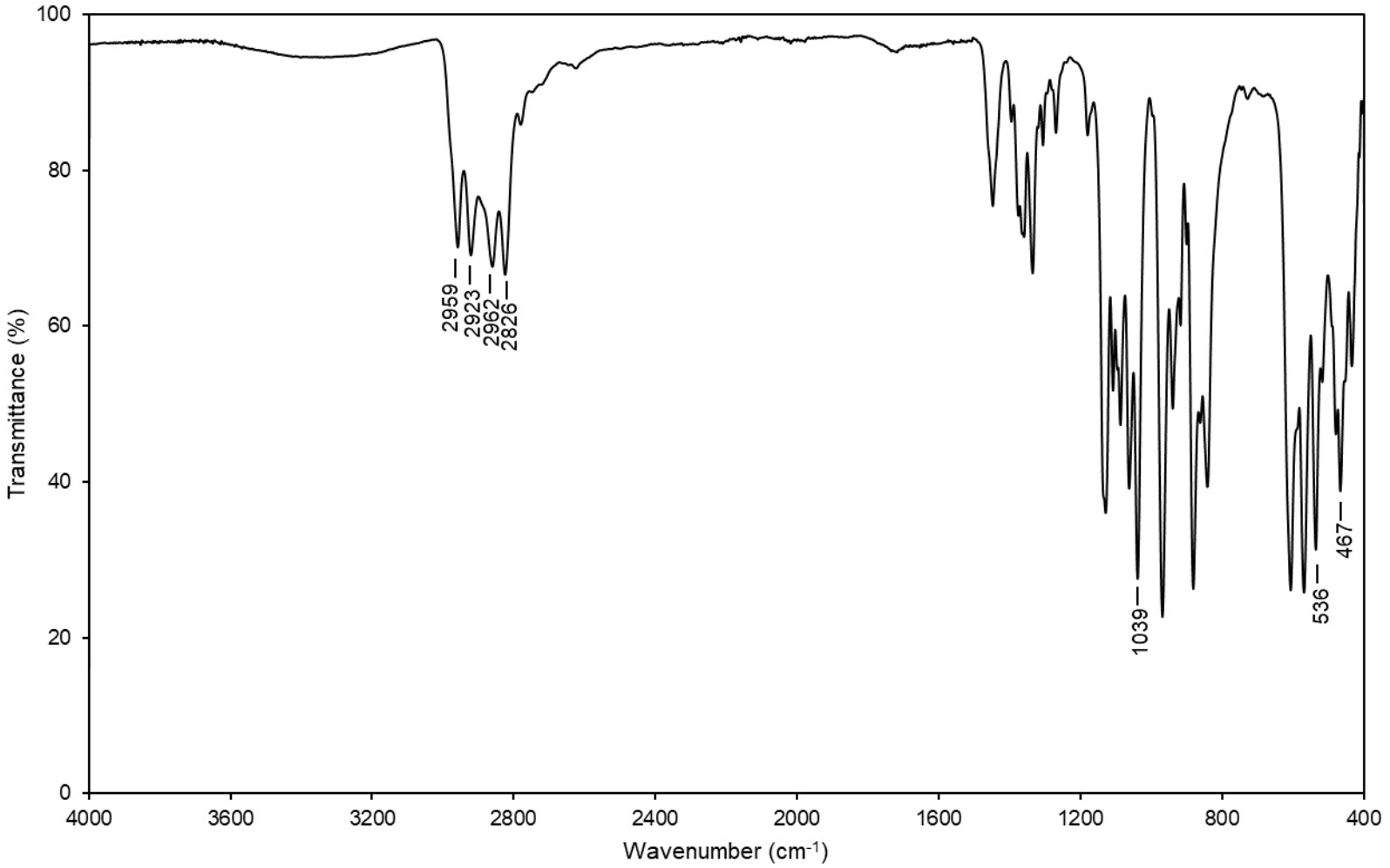

Figure S22. Di-ATR-FTIR Sb-**2**.

S1.6 References

(1) Moaven, S.; Yu, J.; Yasin, J.; Unruh, D. K.; Cozzolino, A. F. Precise Steric Control over 2D versus 3D Self-Assembly of Antimony(III) Alkoxide Cages through Strong Secondary Bonding Interactions. *Inorg. Chem.* **2017**, *56* (14), 8372–8380. https://doi.org/10.1021/acs.inorgchem.7b01049.

(2) Sheldrick, G. M. *SADABS: Programm for Empirical Absorption Correction of Area Detectors*; University of Göttingen, Germany, 1996.

(3) Sheldrick, G. M. SHELXTL Version 2014/7: Programs for the Determination of Small and Macromolecular Crystal Structures by Single Crystal X-Ray and Neutron Diffraction. *Univ. Gött. Ger. URL Httpshelx Uni-Ac Gwdg DeSHELXindex Php* **2014**.

(4) Neese, F. *ORCA – an Ab Initio, Density Functional and Semiempirical Program Package, Version 2.9.0*; Max-Planck-Insitut für Bioanorganische Chemie, Mülheim and der Ruhr, 2013.

(5) van Lenthe, E.; Baerends Evert, J.; Snijders, J. G. No Title. *J Chem Phys* **1993**, *99*, 4597–4610.

(6) Heully, J. L.; Lindgren, I.; Lindroth, E.; Lundqvist, S.; Maartensson-Pendrill, A. M. No Title. *J Phys B Mol Phys* **1986**, *19*, 2799–2815.

(7) Grimme, S.; Ehrlich, S.; Goerigk, L. Effect of the Damping Function in Dispersion Corrected Density Functional Theory. *J. Comput. Chem.* **2011**, *32* (7), 1456–1465. https://doi.org/10.1002/jcc.21759.

(8) Weigend, F.; Ahlrichs, R. Balanced Basis Sets of Split Valence, Triple Zeta Valence and Quadruple Zeta Valence Quality for H to Rn: Design and Assessment of Accuracy. *Phys. Chem. Chem. Phys.* **2005**, *7* (18), 3297–3305. https://doi.org/10.1039/B508541A.

(9) Schafer, A.; Horn, H.; Ahlrichs, R. Fully Optimized Contracted Gaussian Basis Sets for Atoms Li to Kr. *J. Chem. Phys.* **1992**, *97* (4), 2571–2577. https://doi.org/10.1063/1.463096.

(10) Weigend, F. Accurate Coulomb-Fitting Basis Sets for H to Rn. *Phys. Chem. Chem. Phys.* **2006**, *8* (9), 1057–1065. https://doi.org/10.1039/B515623H.

(11) Kohn, W.; Sham, L. J. Self-Consistent Equations Including Exchange and Correlation Effects. *Phys. Rev.* **1965**, *140* (4A), A1133–A1138. https://doi.org/10.1103/PhysRev.140.A1133.

(12) Kendall, R. A.; Früchtl, H. A. The Impact of the Resolution of the Identity Approximate Integral Method on Modern Ab Initio Algorithm Development. *Theor. Chem. Acc.* **1997**, *97* (1), 158–163. https://doi.org/10.1007/s002140050249.

(13) Boys, S. F.; Bernardi, F. The Calculation of Small Molecular Interactions by the Differences of Separate Total Energies. Some Procedures with Reduced Errors. *Mol. Phys.* **1970**, *19* (4), 553–566. https://doi.org/10.1080/00268977000101561.

(14) Lu, T.; Chen, F. Multiwfn: A Multifunctional Wavefunction Analyzer. *J. Comput. Chem.* **2012**, *33* (5), 580–592. https://doi.org/10.1002/jcc.22885.

(15) Nicolay, K.; Braun, K. P. J.; Graaf, R. A. de; Dijkhuizen, R. M.; Kruiskamp, M. J. Diffusion NMR Spectroscopy. *NMR Biomed.* **2001**, *14* (2), 94–111. https://doi.org/10.1002/nbm.686.

(16) Clará, R. A.; Gómez Marigliano, A. C.; Morales, D.; Sólimo, H. N. Density, Viscosity, Vapor−Liquid Equilibrium, and Excess Molar Enthalpy of [Chloroform + Methyl *Tert* -Butyl Ether]. *J. Chem. Eng. Data* **2010**, *55* (12), 5862–5867. https://doi.org/10.1021/je100821g.